Non-Passive Behavior of Equivalent Circuit Components in AC Powder Electroluminescence (ACPEL) Lamps

C. J. Winscom,[z] P. G. Harris, and J. Silver[*]

Centre for Phosphors and Display Materials, Wolfson Centre for Materials Processing, Brunel University, Uxbridge, Middlesex UB8 3PH, United Kingdom

For the first time, the voltage and frequency characteristics of a single layer AC powder electroluminescent lamp have been examined in detail to reveal the individual contributions of the material components involved. Statistical modelling has been employed to refine the equivalent circuit description of the lamp. DC-blocked resistance-capacitance networks can be reduced to a single effective resistance and capacitance in series. The frequency dependence of these two quantities in the range 4–1600 Hz has been used to unravel the behavior of the different underlying resistance and capacitance components at different voltage amplitudes in the range 25–150 V. The resistive contribution, R, of the activated ZnS phosphor is shown to be non-passive, and obeys the form: $R(V,f) = R^0(V).f^{-1/3}.e^{-T.f}$, where V is the applied voltage, f is the frequency and T is a time constant, at all voltages. For both ZnS and $BaTiO_3$, other characteristics indicate the presence of a thinner, non-polarized region within each semiconducting particle located within the particle's crust. A marked change in the characteristics of the different component values occurs between 25 and 50 V, consistent with the onset of light emission, after which smooth changes in all values are observed up to 150 V.

Thick film AC electroluminescence, also referred to as AC powder electroluminescence (ACPEL), can be achieved with a simply-constructed layer structure to produce a surface-distributed light source. The first examples were reported by Destriau in 1936.[1] Today, the use of modern materials[2] allows the structure of the AC electroluminescent device to be reduced to just one active layer between two electrodes; this makes the manufacture of this light source particularly economical. The mechanism of operation of ACPEL devices has been the subject of some debate.[3–5] As the voltage across the sandwich increases, initially no light is emitted until a voltage threshold is exceeded, when it is thought that carriers (holes and electrons) are generated in the phosphor matrix by the applied field. These carriers are swept by the field in opposite directions, before eventually recombination occurs with the emission of light. This may occur both before and after the voltage across the device is reversed. After exceeding the voltage threshold for light emission, further increases in the voltage produce a near linear increase in luminescence.[2]

The economic advantage offered by ACPEL light sources is offset by two main weaknesses: efficacy and longevity, both of which are at least an order of magnitude worse than for the OLED alternative as a surface-distributed light source. In order to tackle efficacy improvement, we believe that a thorough characterization of the ACPEL device is a strategic prerequisite. The purpose of this work, then, has been to derive and characterize a reliable equivalent circuit, and identify as far as possible the contributions which the individual material components make to elements of that circuit. Over the last several decades, ACPEL equivalent circuits ranging from a simple capacitance to more complex passive resistance - capacitance networks[6,7] have been proposed, but have lacked detailed experimental confirmation. In the related field of thin-film AC electroluminescence (TF-ACEL), other equivalent circuits[8–10] have been deduced from experimental charge density-voltage (Q-V) plots, the interpretation of which is the subject of critical debate.[11] TF-ACEL can support volume currents in the continuous ZnS film, whereas in ACPEL any phosphor currents are restricted to the individual dispersed particles,[4] and this may give rise to different effects. We show in the conclusion that these TF-ACEL equivalent circuit variants are not appropriate for our ACPEL device.

Whilst ACPEL devices have essentially capacitive characteristics under zero-field conditions, we have already shown[12] that the simplest "blocked semiconductor" equivalent circuit of a single layer ACPEL device can be reduced to an effective resistance R and capacitance C in series, both of which can then be determined by experiment

as functions of voltage and frequency. In a subsequent study,[13] this simplification was adopted showing that at a constant frequency of 200 Hz, the remarkable changes in the effective series resistance and capacitance as a function of voltage amplitude are brought about directly by the activated ZnS phosphor.

In this report we note that application of AC theory to any circuit formed from an arbitrary network of component resistances and capacitances which is "blocked", i.e. has no direct DC pathway, can always be reduced to an effective resistance-capacitance pair in series. Frequency-voltage mapping of the experimental values of this resistance-capacitance pair then allows reconstruction of the underlying details of the equivalent circuit with the aid of statistical modelling. Examination and refinement of successive circuit choices in a voltage amplitude range 25–150 V and a frequency range 4–1600Hz (sinusoidal waveform) provides the route by which the individual contributions of the material components can be identified. In particular, the resistive element attributed to the emissive phosphor component is shown to exhibit frequency dependence, and is thus considered to be non-passive.

The methodology described in this work allows the detailed electrical characteristics of any AC electroluminescent device to be determined, and provides an alternative to the Q-V plotting approach mentioned earlier. Furthermore, it offers new access to the internal processes occurring in these devices.

Experimental

Device architectures.—Various different ACPEL device architectures are commonly in use;[2] in this study we have chosen a reverse architecture as shown in Figure 1a. The structure comprises a silver electrode deposited on a coated paper base as a bottom layer, a middle layer of phosphor-containing materials and a top layer of a PEDOT/PSS as a transparent conductive electrode. The use of PEDOT/PSS as the transparent electrode has a lower transmission and conductivity than sputtered indium tin oxide (ITO), but offers better integrity in a flexible device.

Materials.—The single layer ACPEL panels were prepared as previously described[2] by first coating a silver ink (AG500 supplied by Nicomatic, UK) backing electrode onto a substrate, typically polyethylene terephthalate (PET), but in this case electronic grade paper (Nano P60, supplied by Printed Electronics Ltd.) was used. A phosphor (GTP Sylvania GG25) in an insulating binder (ethyl cellulose, Sigma-Aldrich) containing an additional dielectric material (barium titanate, Sigma–Aldrich) was then screen-printed onto this

*Electrochemical Society Member.
[z]E-mail: chris.winscom@brunel.ac.uk
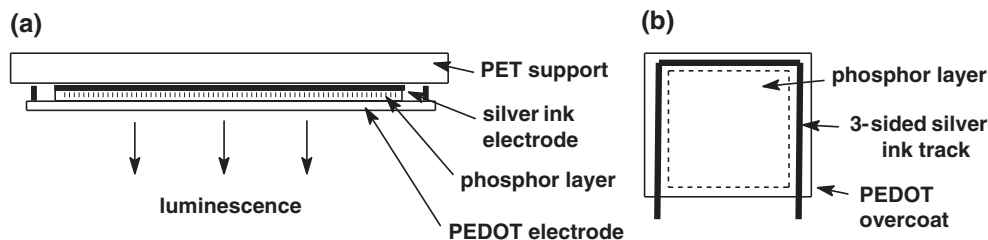
Figure 1. (a) Reverse architecture cross-section of a single layer ACPEL, (b) PEDOT- electrode connection to silver track.

surface. In a typical working single-layer ACPEL the proportions of phosphor(P):dielectric(D):binder(B) are 3:1:4 vol/vol, and the coated thickness of the layer is ca. 30 μm. A 3-sided silver ink track was deposited just outside of the phosphor/backing electrode area. Finally, a layer of PEDOT (Orgacon, supplied by AGFA) was coated over this silver track to provide the transparent electrode. The panels have a cross-section corresponding to that in Figure 1a; the silver connection to the PEDOT overcoat is detailed in Figure 1b.

The active area of the device produced in this way was ca. 43 cm^2. The surface resistivity of silver ink electrodes is typically <1 Ω/square. The PEDOT transparent electrode as coated had a typical surface resistivity of 5.8 $\pm$ 0.5 kΩ/square. The non-operational characteristics of the single layer device are typically a capacitance of 20–35 nF and an unmeasurable (>40 MΩ) DC resistance.

Measurements.—Sinusoidal AC voltages up to $\pm$10 V were provided by a general purpose signal generator (Quantec PSM2200, Newtons4th Ltd.). It also incorporated two isolated voltage measurement channels for measuring true rms voltages, or acting together as a vector voltmeter. The input impedances were both 1 MΩ. An amplifier (Newtons4th Ltd.) was used to deliver up to $\pm$150 V amplitude in the range 4–1600 Hz. The arrangement for monitoring voltage amplitudes and phase shifts to determine the effective C and R under different sinusoidal AC conditions has been described previously.[13]

For the lamp area (84 $\times$ 54 mm) covered by the transparent electrode in contact with the 3-sided (84-54-84 mm) silver track, it became important to have an upper limit estimate of the contribution of this structure to the electrode resistance. This is difficult to estimate theoretically in relation to the surface resistivity (ρ_s). We adopted the following experimental approach: PEDOT coatings on a "soft" substrate having a similar surface resistivity were produced, and a 3-sided wire electrode (80 $\times$ 50 mm) placed in contact with it under an even pressure to provide a uniform contact. A regularly spaced array of 19 $\times$ 9 contacts (total contact area <5% of the PEDOT area) was placed within the bounded area under an even pressure. To simulate a device in a low impedance regime (e.g. at frequencies >1000Hz) all array contacts were connected together. The resistance between the 3-sided electrode and the array electrode was measured and found to be ca. ρ_s/6. We reason that 1 kΩ is therefore a generous upper limit of the electrode resistance for the lamp construction used in this study.

Software.—To gain insight into the general behavior of different models specific software was written to simulate the effective resistance and capacitance pair data for a number of different equivalent circuit variations over the 4–1600 Hz frequency range. Both passive and non-passive behavior of the underlying trial R- and C-component contributions (without optimization) could be examined in an exploratory way.

For models which could not readily be eliminated at this preliminary stage, a more sophisticated software was written, where starting values were estimated from the experimental data and were optimized using a statistical modelling approach. At each of the six voltages, the 19 experimental C, R pairs are related. However, all models examined exhibit "blocked" DC behavior, and it is straightforward to show that the functional form of C will always contain at least one independent parameter (see e.g C_d in Equations 3 and 4, in the simplest variation)

not contained in the functional form of R. These quantities are therefore not transformable, and are handled as 38 independent items of data associated with 19 frequencies. It was considered inadmissable to use models involving the variation of more than 38/3 $\sim$ 12 parameters to minimize the error between model and experiment, so software for examining different equivalent circuit models with up to this number of parameters was written. The basis for optimization was the cumulative improvement of the Coefficient of Determination, $\Re^2$,[14] toward its theoretical maximum value of 1. $\Re^2$ is an established statistical quantity whose purpose is to provide a measure of how well observed outcomes are replicated by a model and is the widely accepted function of choice for optimization of hypothetical models. There are several equivalent definitions; the computationally pragmatic choice is given by

$$\Re^2 = 1 - \left\{ \sum \left(x_i^{expt} - x_i^{model} \right)^2 / \sum \left(x_i^{expt} - x^{av} \right)^2 \right\} \qquad [1]$$

where x_i^{expt} and x_i^{model} are the experimental and modelled values of an observable x, $1 \leq i \leq n$, and x^{av} is the mean value:

$$x^{av} = (1/n) \sum x_i^{expt} \qquad [2]$$

$\Re^2$ for the modelled- vs. experimental values of $\log_{10}$ R, and C, as functions of $\log_{10}$ f, were improved using a gradient ascent variation of the "steepest descents method".[15] The functional search spaces of $\Re^2(\log_{10}$ R) and $\Re^2$(C) have the same number of dimensions, and simultaneous optimization was achieved using the sum of these quantities, which was maximized by calculating the vector derivative of this functional to determine the ascent direction. Convergence of the process was monitored via the 1st and 2nd derivative of the $\Re^2$-sum with respect to iteration cycle. Careful stepping strategies allow lower local maxima in $\Re^2$ to be bypassed, as monitored by the derivatives on a cycle-by-cycle basis.

Specific to this work, it has been known for many decades that passive circuits containing only resistive and capacitive elements (i.e. no accompanying inductance) will not contain the sharper features associated with resonances. Nevertheless, our raw R and C data spans eight octaves of frequency where, R_{eff} spans 3 orders of magnitude, and C_{eff} exhibits a steep gradient at very low frequencies, and these features present an exacting requirement for model refinement by fitting techniques.

Results and Discussion

Whilst the effective R and C observed experimentally are functions of the underlying resistive and capacitive components and frequency (see Equations 3 and 4), it cannot be assumed that the underlying components themselves are entirely passive with respect to voltage and frequency. A previous report[12] considered the most primitive form of equivalent circuit involving a purely dielectric capacitive component in series with a second component comprising a parallel capacitance/resistance (see Figure 2) representing the effects of all other dispersed materials. The relationship is given by:

$$R = R_e + R_a / \left(1 + W_a^2 \right) \qquad [3]$$
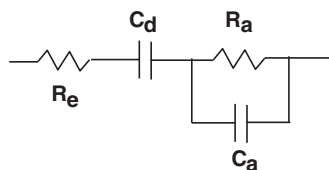
Figure 2. The simplest model of components underlying the effective R and C observed.

$$1/C = (1/C_d) + (1/C_a) \cdot W_a^2 / \left(1 + W_a^2 \right) \qquad [4]$$

where $W_a = \omega C_a R_a$ and ω is the angular frequency (radians s^{-1}), and R_e is the electrode resistance. Equations 3 and 4 relate these components to R and C which can be easily determined experimentally.

It was noted[4] that R and C were dependent mainly on applied voltage, but also seemed to have an underlying frequency dependence other than that resulting from the W-terms. To properly address the subsequent problem of efficacy, lamp operation advantageously employing waveforms other than sinusoidal must be explored. Higher frequency components are then present, and the true dependence of the effective R and C must first be understood. Considering the simplest representative circuit (Fig. 2) in a regime where $\omega^2 C_a^2 R_a^2 \gg 1$, and $R_a \gg R_e$ (10–200 Hz) Equation 1 approximates to $R \approx 1/\omega^2 C_a^2 R_a$, a typical log (R) vs. log (f) plot should have a gradient of –2. Figure 3 shows the corresponding plot for the frequency range 4 to 1600 Hz.

Clearly, the gradient in question is closer to –1 for all voltages in the 25–150 V range, indicating that the product $C_a^2 R_a$ is additionally dependent on frequency. (The intermediate voltages 25, 75 and 125 V have been omitted to avoid congestion, but show the same trend.) To assess the behavior of the effective capacitance, C, we note that its variation with frequency (ca. 2x over 4–1600 Hz) at any voltage is much less than for the effective resistance. For an entirely passive behavior, Equation 4 requires that at high frequencies where the $W_a^2/(1+W_a^2)$ terms tend to unity, C should become constant according to the asymptotic value $1/C = (1/C_d) + (1/C_a)$. A straightforward plot of 1/C vs. frequency in Figure 4 demonstrates the marked lack of dependence for frequencies ≥ 200 Hz, ($\leq 5\%$ change from 200–1600 Hz for all voltages ≥ 50 V).

Any significant non-passive behavior in C should be markedly evident over this 3-octave range; its absence indicates that any frequency dependence of the component capacitive elements of the ACPEL device is slight. Together with the result from the $\log_{10}$ R vs. $\log_{10}$ f behavior, we conclude that the resistive circuit component exhibits the more pronounced frequency-dependent behavior.

The electrode resistance, R_e, is determined to be ≤ 1 kΩ, as explained in the Experimental section. However, at high frequencies,
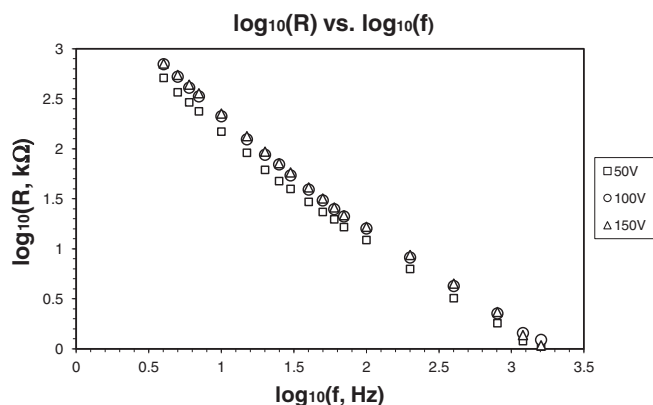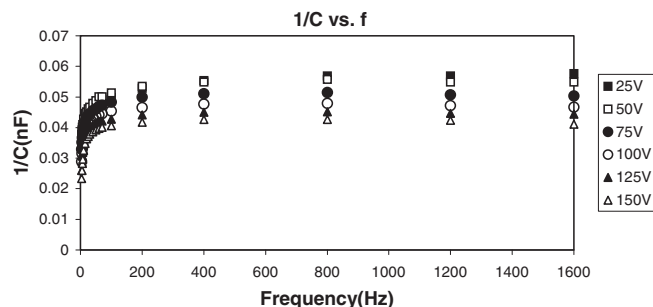
Figure 4. 1/C vs. frequency over the range 4 to 1600 Hz at different voltages.

the experimentally observed resistance range approaches this upper limit. We therefore consider R_e to be a parameter under optimization. If we subject the simple model in Figure 2 to statistical analysis using simple frequency dependencies:

$$R_a = R_a^0 \cdot f^{mra} \qquad [5]$$

$$C_a = C_a^0 \cdot f^{mca} \qquad [6]$$

and allow the 6 parameters R_e^0, R_a^0, mr_a, C_a^0, mc_a and C_d to be optimised, the result summarized in Table I is obtained.

Experience shows that models must achieve values of $\Re^2 > 0.99$ for both plots before being considered plausible. The plots of the Log R- and C experimental points superimposed on their respective curve fits show that the values of $\Re^2$ (log R) and $\Re^2$(C) visually achieve a borderline acceptability. Nevertheless, mr_a is reasonably consistent across the voltage range, and mc_a is much smaller in magnitude in agreement with the characteristics deduced from the results shown in Figures 3 and 4.

Overall, this first attempt suggested that minor variations of the arrangement might achieve an improvement. Firstly, most of the values of R_e exceed the upper limit determined independently earlier. Moreover, R_e is not constant but tends to track the R_a parameter across the voltage range. This suggests that a small fraction (x_a) of the resistance R_a should not to be bridged by its associated capacitance C_a, thereby providing an additional series resistance component larger than that provided solely by R_e. In addition, it has already been established that R_a and C_a are mainly determined by the phosphor material.[13] This suggested the inclusion of an additional passive parallel R_b and C_b arrangement in series with R_a and C_a to reflect the effect of other components (e.g. BaTiO$_3$) in the phosphor layer. The model shown in Figure 5 incorporates these improvements and requires optimization of 9 parameters.

The results of this optimization are presented in Table II.

The three additional parameters (R_b, C_b, x_a) are all needed to deliver the improvement in $\Re^2$ across the range; visually, too, the curve fits become more acceptable. R_e is reasonably constant across the voltage range, well within the upper limit estimate discussed earlier. Apart from the lowest voltage, both mr_a and x_a are very consistent

Figure 3. $\log_{10}$ R vs. $\log_{10}$ f plot over the range 4 to 1600 Hz at different voltages. (25 V, 75 V and 125 V data have been omitted to avoid congestion.).

Table I. Analysis of the ACEL lamp, according to the 6-parameter model circuit in Figure 2.

	25 V	50 V	75 V	100 V	125 V	150 V
R_e (kΩ)	0.780	0.950	1.230	1.380	1.520	1.400
R_a^0 (kΩ)	921	1993	2770	3166	3364	3066
C_a^0 (nF)	93.6	48.7	34.0	28.9	27.1	26.8
C_d (nF)	32.9	38.1	58.6	97.0	173.8	213.6
mr_a	−0.418	−0.543	−0.538	−0.523	−0.504	−0.409
mc_a	−0.136	−0.053	−0.022	−0.011	−0.009	−0.001
$\Re^2$(log R)	0.991	0.994	0.993	0.991	0.990	0.988
$\Re^2$(C)	0.991	0.992	0.994	0.995	0.995	0.994
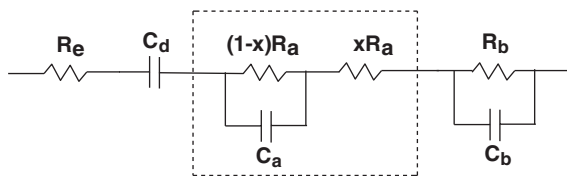
Figure 5. Variation of the simple model described by 9-parameters.

across the range, with mc_a becoming insignificant at higher voltages. It is difficult to reconcile an mr_a value of ca. -0.4 with a physical mechanism and this coarse single-parameter to accommodate departure from a passive R_a was a pragmatic choice, rather than one borne from physical insight. However, there are many physical mechanisms which might account for an $f^{-1/3}$ or $f^{-1/2}$ dependence; exponent values which bracket the consistent mr_a value obtained. It was considered useful to explore modified functions of frequency involving $f^{-1/3}$ and $f^{-1/2}$. One of these variations was found to bring a marked improvement:

$$R_a = R_a^o.f^{-1/3} \exp(-\tau.f) \quad [7]$$

whereby mr_a is now replaced by the time constant, τ, as the parameter being optimized. The rationalization underpinning this intuitive choice is as follows: conductivity is proportional to the density of unquenched charge separation and the rate of charge separation is expected to be proportional to frequency. Preferential carrier mobility along a specific direction in the phosphor particles which are randomly oriented would reduce the effective charge separation rate along the direction of the field to $\sim(f^-)^{1/3}$. Resistance is inversely proportional to conductivity, which is nicely consistent with the $(f)^{-1/3}$ dependence. Quenching processes causing charge recombination also lead to a reduction of conductivity i.e. an increase in resistance. We envisage an exponential term which increases as the characteristic time (τ) for quenching decreases, relative to the time $(1/f)$ to produce charge separation, i.e. $\exp(-\tau.f)$. We note that when $\tau \sim 1$ mS this term has little effect until frequencies become ≥ 1 kHz.

In addition:

$$C_a = C_a^0.f^{mca} \quad [8]$$

is retained, but note that $mc_a = 0$ for voltages >50 V. Table III presents the result of the choice given by Equation 7. It shows significant improvements in $\Re^2(\log R)$ and $\Re^2(C)$ across the voltage range; mostly achieving 0.999 to 3 decimal places. The time constant, τ, is also shown to have a reasonably constant value across the voltage range, and may be fixed at its mean value without impairing values of $\Re^2$. Also, R_e is approximately constant across the voltage range with a value of 501 ± 83 Ω, and again well within the upper limit estimate discussed earlier. R_e can also be given this fixed value without impairing $\Re^2$. The number of parameters in a subsequent model can thus be effectively reduced.

The model described by the circuit in Figure 5 leads to an adequate fit, and suggested that the assignment of discrete electrical identities

to the individual material components of the lamp might be possible. To attempt such a rationale we first examined a structure identical to that of the ACEL lamp in which the phosphor is absent, and found that this could be analyzed with a simple 4-parameter model: R_u, C_u, C_{du}, x_u, the "u" subscript denotes the absence of ZnS phosphor in the structure. This shows that the components in this case turn out to be entirely passive, so that the corresponding mr_u and mc_u parameters are both zero. R_e is now taken to be the average value of that in Table III (501 Ω) without loss of accuracy in determining R_u, C_u, C_{du}, x_u. Table IV presents the results of this analysis.

The values of $\Re^2(\log R)$ and $\Re^2(C)$ indicate that the simple equivalent circuit involving only passive components provides an excellent fit at all voltages. We have previously shown[13] that a similar structure using the insulating binder without added $BaTiO_3$ is simply represented by a single capacitance, on the order of 2–3nF, as expected from a material of low dielectric constant for these dimensions. Formally, $BaTiO_3$ is an intrinsic semiconductor, but in the ACEL lamp structure it functions as a dielectric with a high dielectric constant. Parameters involving the resistive element (R_u and x_u) can therefore be clearly associated with the inclusion of the $BaTiO_3$ semiconductor, as can the capacitive contribution C_u. The capacitive contribution C_{du} seems to be associated with both the binder and the $BaTiO_3$, and the interface between them.[16]

Returning to a lamp structure which contains the phosphor, there is a generalized form of the reduction to a single effective R and C. Figure 6a shows a series concatenation of parallel R_j, C_j components terminated by a simple capacitance. This arrangement is a generalisation of the simpler version shown in Figure 2; it is straightforward to show that the relationship to the effective R and C of this arrangement has the form:

$$R = \Sigma_j R_j / \left(1 + W_j^2\right) \quad [9]$$

$$1/C = (1/C_D) + \Sigma_j \left(1/C_j\right).W_j^2/\left(1 + W_j^2\right) \quad [10]$$

where $W_j = \omega C_j R_j$. Figure 6b shows the effect of added parallel components. Although the expressions are more complicated, this arrangement, too, can be reduced to a single effective resistance and capacitance in series.

In the model represented by Figure 5, the additional $\{R_b, C_b\}$ are confirmed to be of a corrective nature (*cf.* Table II). We now draw on the results in Tables II, III and IV, and make the following observations. Phosphor particles whose average size is ca. 25 μm diameter and the barium titanate of ca.1 μm diameter are embedded in an insulating ethyl cellulose binder to form a layer of ca. 30 μm. In a simplified way, we imagine a layer of close-packed cylindrical elements, each containing a single spherical phosphor particle and embedded in an insulating medium (ethyl cellulose) containing much smaller $BaTiO_3$ particles (see Figures 7a and 7b). Within each cylinder, an insulating binder $+ BaTiO_3$ layer between the phosphor and respective electrodes is present. The interstitial space, which accounts for approximately 10% of the volume of the phosphor cylinders, and thus covers the same fraction of the total electrode area, is filled with

Table II. Analysis of the ACEL lamp, according to the 9-parameter model circuit in Figure 2.

	25 V	50 V	75 V	100 V	125 V	150 V
R_e (kΩ)	0.334	0.437	0.431	0.394	0.359	0.275
R_a^0 (kΩ)	918	1717	2399	2708	2822	2793
C_a^0 (nF)	90.0	49.7	33.7	29.9	28.2	27.8
R_b (kΩ)	9.3	11.0	8.8	7.7	5.7	5.2
C_b (nF)	200.7	183.4	194.9	251.5	299.3	357.2
C_d (nF)	34.5	38.8	33.7	98.0	158.4	262.7
mr_a	-0.277	-0.408	-0.409	-0.408	-0.400	-0.401
mc_a	-0.107	-0.026	-0.000	-0.000	-0.000	-0.000
x_a	$4.97.10^{-3}$	$8.23.10^{-3}$	$7.72.10^{-3}$	$8.03.10^{-3}$	$7.97.10^{-3}$	$7.98.10^{-3}$
$\Re^2(\log R)$	0.995	0.997	0.997	0.996	0.996	0.993
$\Re^2(C)$	0.993	0.998	0.999	0.998	0.998	0.997

Table III. Analysis of the ACEL lamp, using a 9-parameter model with modified frequency dependence of R_a (bracketed values are fixed, see text).

	25 V	50 V	75 V	100 V	125 V	150 V
R_e (kΩ)	0.374	0.536	0.583	0.566	0.550	0.399
$R_a{}^0$ (kΩ)	1349	1585	1996	2260	2381	2390
$C_a{}^0$ (nF)	86.9	50.5	35.8	31.9	30.0	29.4
R_b (kΩ)	9.6	12.7	10.4	10.0	8.2	7.9
C_b (nF)	324.8	168.7	177.9	218.8	256.9	295.1
C_d (nF)	36.8	39.3	57.0	86.4	127.6	196.8
τ (s)	$9.49 \cdot 10^{-4}$	$1.01 \cdot 10^{-3}$	$1.03 \cdot 10^{-3}$	$1.13 \cdot 10^{-3}$	$1.15 \cdot 10^{-3}$	$1.28 \cdot 10^{-3}$
mr_a	$(-1/3)$	$(-1/3)$	$(-1/3)$	$(-1/3)$	$(-1/3)$	$(-1/3)$
mc_a	-0.124	-0.027	0	0	0	0
x_a	$7.99 \cdot 10^{-3}$	$1.04 \cdot 10^{-2}$	$1.11 \cdot 10^{-2}$	$1.22 \cdot 10^{-2}$	$1.26 \cdot 10^{-2}$	$1.36 \cdot 10^{-2}$
$\Re^2(\log R)$	0.996	0.999	0.999	0.999	0.999	0.999
$\Re^2(C)$	0.993	0.998	0.999	0.999	0.999	0.999

Table IV. Analysis of the lamp structure without phosphor using a 4-parameter model circuit (see text). Bracketed values are fixed at their average value determined previously.

|	25 V	50 V	75 V	100 V	125 V	150 V
R_e (kΩ)	(0.501)	(0.501)	(0.501)	(0.501)	(0.501)	(0.501)
R_u (kΩ)	8283	4124	2743	2126	1781	1525
C_u (nF)	3.7	3.7	3.7	3.7	3.7	3.7
C_{du} (nF)	203.4	163.7	550.5	798.2	1485	1671
x_u	$4.04 \cdot 10^{-4}$	$9.39 \cdot 10^{-4}$	$1.35 \cdot 10^{-3}$	$1.78 \cdot 10^{-3}$	$2.24 \cdot 10^{-3}$	$2.67 \cdot 10^{-3}$
$\Re^2(\log R)$	0.998	0.999	0.999	0.999	0.999	0.999
$\Re^2(C)$	0.998	0.999	0.999	0.999	0.999	0.999

binder + $BaTiO_3$ only. One can envisage the electrical characteristics being an integration of all such cylindrical and interstitial elements over the electrode area (see Figure 7).

A realistic representation of the lamp would then be the circuit shown in Figure 7c. Identifying C_{di}, C_i and R_i with the interstitial binder + $BaTiO_3$ composition, these parameters will be related to the parameters of the structure without phosphor by: $C_{di} = y_i.C_u$, $C_i = y_i.C_u$ and $R_i = R_u/y_i$, where $y_i \sim 0.1$ is the fraction of the electrode area covered by the interstitial regions. The estimated parallel contribution of the interstitial region ($C_{di} = 16–160$ nF, $C_i \sim 0.3$ nF, $R_i \sim 15–82$ MΩ) is that of a correction only, compared with the effect of the "cylinders" region. In the right hand arm in Figure 7c, representing the "cylinders", the two blocking capacitances associated with the phosphor and insulating layers act as their serial combination and cannot be separately optimized. Although it is tempting to suggest that C_b, R_b might be related to C_u, R_u in a similar fashion, the analogy is not straightforward. A numerical integration, using the approximate dimensions of the layer, show that the optimized R_b is at least an

order of magnitude smaller than expected. However, this thin insulating layer will be most prone to both absorbed atmospheric moisture from above, and dendritic migration of silver into binder under the influence of an electric field[17] from below. Also, in an electric field, the ferroelectric character of the $BaTiO_3$ in the thin insulating layer between phosphor and silver causes movement of the particles within the layer,[18] which may also contribute to the reduction of this resistive component. Clearly, an additional dielectric layer could provide better insulation protection, but the single layer design here delivers optimum light output.

We conclude that R_a can be identified with the phosphor and a passive R_b with the $BaTiO_3$. The corrective nature of the "i" and "b" components put forward here nicely explain why the simpler model in Figure 6a performs so well. It is reasonably straightforward to include such corrections in the parameter optimization scheme. By utilising the binder + $BaTiO_3$ data, the interstitial correction would introduce one extra parameter (y_i) over that in Figure 6a. However, the practical drawback when optimising small corrections is that such parameters vary in very shallow minima; convergence is very slow and accuracy is poor. We prefer to set the parameter y_i at 0.1; any minor deviation from this position will not introduce significant errors in determining the phosphor parameters. Further, R_b and C_b are retained as separately optimized parameters, where R_b, C_b are passive components and R_b takes exactly the same fractional R-partition as R_i (i.e. x_u in Table IV). R_e takes the fixed value of 501 Ω. We note too that at 75 V and above, mc_a could also be fixed at zero with the further reduction of one parameter. However, we choose to retain this to best accommodate the 25–75 V threshold region. The final model in Figure 8 then contains just seven parameters for optimization.

The new parameter set may be optimized and the results are shown in Table Va. The $\Re^2(\log R)$ and $\Re^2(C)$ in Table Va confirm the high degree of correlation between model and experiment. Table Vb presents the results of the reverse process in which the parameters taken from Table Va are used to simulate a noise-free set of (R, C) data according to the model in Figure 8. Recovery of the parameters using the statistical modelling process is presented in Table Vb. Very low discrepancy levels relative to Table Va illustrate the errors to be expected from this
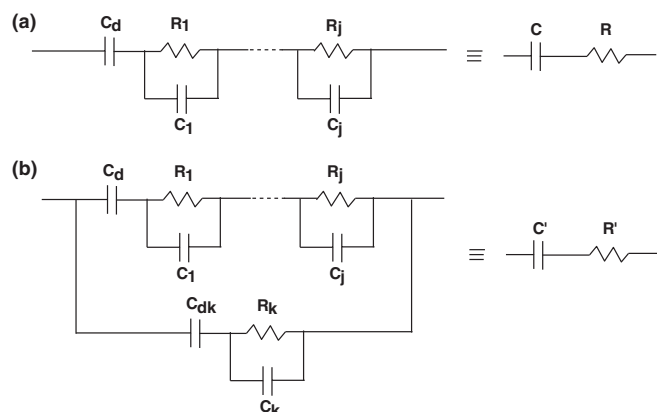
Figure 6. (a) Serial concatenation of R_j, C_j-components, (b) effect of added parallel components.

(a)
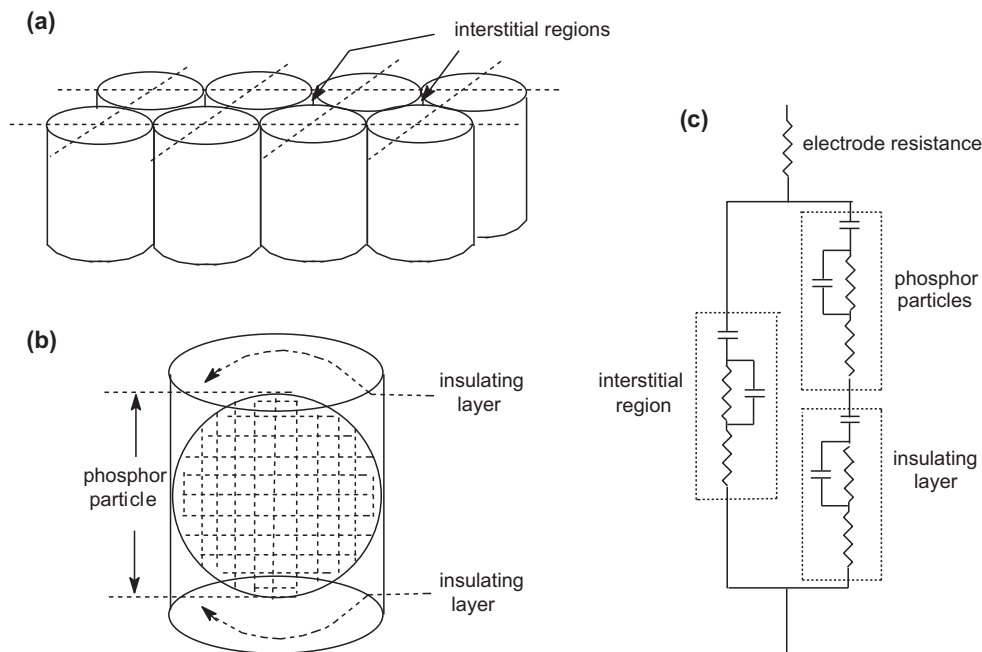
Figure 7. (a) A simplified regular arrangement of cylindrical cross-sections, (b) individual cylinder containing a phosphor particle element and its associated insulating layer, (c) representative circuit components after integrating over the distinct regions.

Table V. (a) Analysis of the ACEL lamp, according to the 7-parameter model circuit in Figure 8 (bracketed values are fixed).

	25 V	50 V	75 V	100 V	125 V	150 V
R_e (kΩ)	(0.501)	(0.501)	(0.501)	(0.501)	(0.501)	(0.501)
R_a^0 (kΩ)	1244	1667	1968	2166	2339	2387
C_a^0 (nF)	91.8	52.3	37.7	34.2	32.2	31.3
R_b (kΩ)	10.2	13.5	11.2	10.3	9.5	9.4
C_b (nF)	279.6	169.3	168.4	209.2	239.7	273.1
C_d (nF)	34.9	38.0	51.2	69.8	95.9	134.4
τ (s)	$(1.092.10^{-3})$	$(1.092.10^{-3})$	$(1.092.10^{-3})$	$(1.092.10^{-3})$	$(1.092.10^{-3})$	$(1.092.10^{-3})$
mr_a	$(-1/3)$	$(-1/3)$	$(-1/3)$	$(-1/3)$	$(-1/3)$	$(-1/3)$
mc_a	−0.129	−0.034	−0.000	−0.000	−0.000	−0.000
x_a	$6.78.10^{-3}$	$1.10.10^{-2}$	$1.29.10^{-2}$	$1.42.10^{-2}$	$1.44.10^{-2}$	$1.38.10^{-2}$
$\Re^2(\log R)$	0.995	0.999	0.999	0.999	0.999	0.999
$\Re^2(C)$	0.993	0.998	0.999	0.999	0.999	0.999

type of multidimensional solution process. In this case the error levels are typically only a few %, leading to confidence in the quantitative trends across the voltage range. Moreover, the consistent replication of the parameter values in Table Va by those in Vb over such wide voltage range provides additional confidence that unambiguous solutions have been obtained.

The results in Table Va show that the overall changes in the parameters compared with Table III are small, with no deterioration in $\Re^2(\log R)$ and $\Re^2(C)$, and confirm that the characteristics of the lamp are mainly determined by the phosphor-containing "cylinders". The three dominant phosphor–related parameters R_a^0, C_a^0, and C_d each vary smoothly through the voltage range. From these

Table V. (b) Recovery of parameters of the ACEL lamp, after simulation using the data of Table Va in the 7-parameter model circuit in Figure 8 (bracketed values are fixed).

|	25 V	50 V	75 V	100 V	125 V	150 V
R_e (kΩ)	(0.501)	(0.501)	(0.501)	(0.501)	(0.501)	(0.501)
R_a^0 (kΩ)	1181	1609	1953	2140	2331	2362
C_a^0 (nF)	94.2	53.1	37.8	34.4	32.3	31.5
R_b (kΩ)	10.0	13.2	11.0	10.2	9.7	9.5
C_b (nF)	285.3	170.2	169.7	210.6	238.7	273.3
C_d (nF)	34.5	37.5	50.9	68.8	95.2	131.1
τ (s)	$(1.092.10^{-3})$	$(1.092.10^{-3})$	$(1.092.10^{-3})$	$(1.092.10^{-3})$	$(1.092.10^{-3})$	$(1.092.10^{-3})$
mr_a	$(-1/3)$	$(-1/3)$	$(-1/3)$	$(-1/3)$	$(-1/3)$	$(-1/3)$
mc_a	−0.131	−0.033	−0.002	0.000	0.000	0.000
x_a	$7.00.10^{-3}$	$1.15.10^{-2}$	$1.31.10^{-2}$	$1.45.10^{-2}$	$1.45.10^{-2}$	$1.40.10^{-2}$
$\Re^2(\log R)$	1.0000	1.0000	1.0000	1.0000	1.0000	1.0000
$\Re^2(C)$	1.0000	1.0000	1.0000	1.0000	1.0000	1.0000
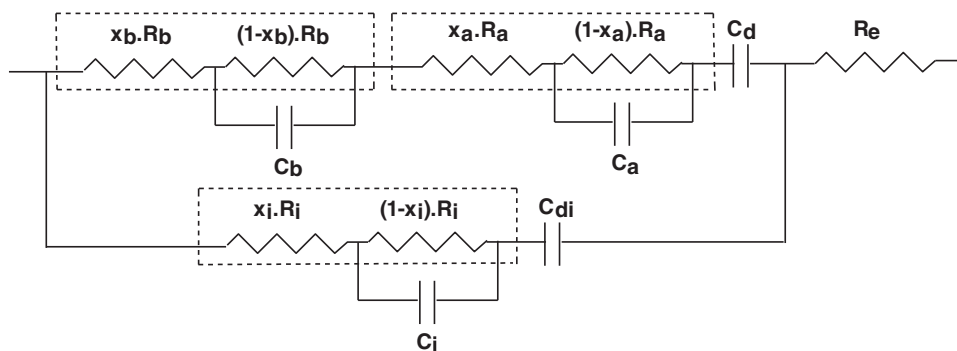
Figure 8. The final model which reduces to 7 parameters. The correction for the interstitial components (i) are values derived from an identical structure containing no phosphor (see text).The remaining seven parameters under optimization are: C_d, R_a^0, C_a^0, x_a, mc_a, R_b, C_b.

parameters, explicit formulae for each of them can be derived to describe the detailed behavior of the phosphor with respect to voltage. However, their derivation and inclusion requires an extended discussion beyond the scope of this report.

To provide a visual comparison of the typical fitting quality, the R- and C-dependencies on frequency predicted by the parameters of the model at 75 V (Table Va) are compared with the experimental values at this voltage in Figure 9. (Supplementary material is available to allow comparison at the other voltages.)

Conclusions

For the first time different equivalent circuit models for a single layer powder ACEL lamp have been explored and analyzed with the
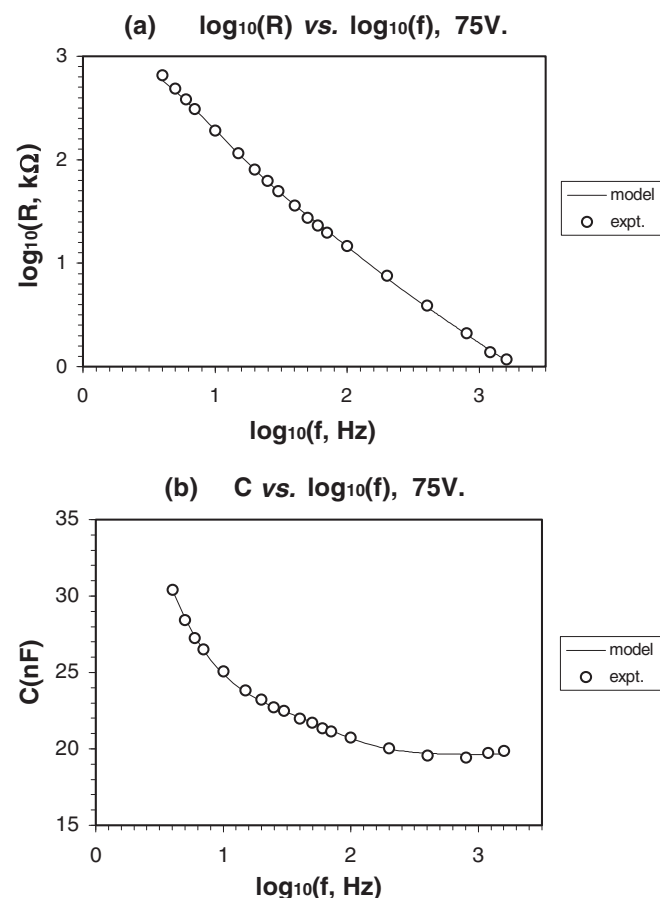
Figure 9. Comparison of model simulation with experimental values at 75 V of (a) $\log_{10}$ R and (b) C (see text).

aid of statistical modelling using extensive experimental data in the frequency range 4–1600 Hz and voltage amplitude range 25–150 V. Evidence has been presented that the model shown in Figure 8 provides a consistent description by identifying (R_a, C_a) with the phosphor component, (R_i, C_i) and (R_b, C_b) with the BaTiO$_3$ semiconductor, whilst C_d and C_{di} are dependent on the insulator-semiconductor mixtures in a less distinct way. The resistive component associated with phosphor, R_a, is active in the sense that it is markedly frequency dependent. The functional form given by Equation 7 brings about a significant improvement in fitting across the 25–150 V range studied. Choice of this functional form was rationalized in terms of preferential carrier mobility along a specific direction in the phosphor particles which are randomly oriented, and the generation of charge separation ($\sim$f) against the lifetime of traps ($\sim\tau$) able to quench by recombination.

At the lowest voltage 25 V (17.7 Vrms) the capacitance C_a also exhibits a frequency dependence which becomes insignificant at higher voltages. We note that there is a marked change in the key parameters in Table Va between 25 and 50 V, consistent with the threshold voltage for onset of light output. In contrast to the ACEL lamp, a device structure where the phosphor is completely absent conforms to the simplest equivalent circuit (see Figure 2) in which all the components are passive.

The smooth variation of the dominant phosphor–related parameters R_a^0, C_a^0, and C_d with respect to voltage can be used to describe the behavior of the phosphor as a function of voltage in detail warrants a lengthier discussion, but is not included in this report. Notably, however, the experimental frequency-voltage mapping approach used here to explore the characteristics stands in contrast to the charge density-voltage plotting approaches typically used for TF-ACEL devices.[8–11] These approaches deduce equivalent circuit variants similar to that in Figure 2, where the resistance R_a is replaced by two juxtaposed Zener diodes. These circuits require a *decrease* in this resistance to a plateau as voltage is increased. Our results for a powder device (both the experimental R_{eff} at any fixed frequency, and the parameter (R_a^0 in Tables I, II, III, V) clearly demonstrate that an *increase* to a plateau occurs. When the phosphor is removed, however, and the structure contains only a non-emissive semiconductor (BaTiO$_3$) in a binder, the trend reverses (R_u in Table IV). Clearly, it would be interesting to apply the frequency-voltage mapping techniques described herein to thin film devices.

A particular feature revealed in this study is that both semiconductor materials, regardless of their relative size difference, exhibit a small significant fraction (on the order of 0.1–1%) of their internal resistance not bounded by an associated capacitance. Assuming a field-dependent semi-conductivity within each particle, this feature implies the presence of a thinner, non-polarized region within each particle, located presumably within its crust. This is an important observation for the phosphor particles, since it suggests that the Grezkoviak and Winkel observation[19] (emission from centers only in the thin ZnS-crust) and the Brunel group observation[20] (successive etching shows emitting centres can exist throughout),

although seemingly contradictory at first sight,[5] might indeed be in accordance.

The modelling itself is useful from a design standpoint since for the first time it gives insight into the effect of each component in the single layer. How particles of a different dimension might affect performance characteristics of the lamp, and how semiconductors like the ZnS phosphor and $BaTiO_3$ in an insulating medium behave in an alternating external electric field, are two examples of where lamp design can be aided. Not only does the analysis of electrical characteristics described in this work provide a good probe of the internal mechanisms in activated zinc sulfide crystals, it is also a prerequisite to studying the question of ACPEL lamp efficacy, where different waveforms will be composed of different frequency components. Finally, it has been demonstrated that the statistical modelling approach, though tedious, can provide a reliable methodology for electrically characterising AC-driven devices.

Acknowledgments

References

1. G. J. Destriau, *Chim. Phys.*, **33**, 587 (1936).
2. R. Withnall, J. Silver, P. G. Harris, T. G. Ireland, and P. J. Marsh, *J. SID*, **19**(11), 798 (2011).
3. H. F. Ivey, "*Electroluminescence and related effects*", p. 101, Academic Press, New York (1963).
4. M. Bredol and H. S. Dieckhoff, *Materials* **3**, 1353 (2010).
5. C. J. Winscom, R. Withnall, and J. Silver, "*Chapter 13: Thick Film AC Electroluminescence*" in *Handbook of Digital Imaging*, Vol. **3**, p. 655, ed. M. Kriss, Wiley and Sons Ltd. (2015).
6. J. R. MacDonald, *Phys. Rev.*, **92**, 4 (1953).
7. K. Sh. Enikeeva, *Soviet Physics Journal*, **1**, 75 (1966).
8. Y. S. Chen and D. C. Krupka, *J. Appl. Phys.* **43**, 4089 (1972).
9. D. H. Smith, *J. Lumin.* **23**, 209 (1981).
10. P. M. Alt, *Proc. SID*, **25**, 123 (1984).
11. J. C. Hitt, J. P. Bender, and J. F. Wage, *Critical Reviews in Solid State and Material Sciences*, **25**(1), 29 (2000).
12. C. J. Winscom, P. G. Harris, and J. Silver, *SID Symposium Digest* **45**(1) 1301 (2014).
13. C. J. Winscom, P. G. Harris, and J. Silver, *ECS JSS* **3**(6) R104 (2014).
14. See e.g. S. A. Glantz and B. K. Slinker, "*Primer of Applied Regression and Analysis of Variance*" p. 248, McGraw Hill Inc., New York (1990). *Note added in proof* : the Wikipedia entry under "Coefficient of Determination" also provides a helpful introduction.
15. W. H. Press, B. P. Flannery, S. A. Teukolsky, and W. T. Vetterling, "*Numerical Recipes*", p. 301, Cambridge University Press, Cambridge (1986).
16. M. Tyunina and J. Levoska, *Applied Physics Letters* **88**, 262904 (2006).
17. S. J. Krumbein, "*Metallic Electromigration Phenomena*", *33rd Meeting IEEE Holm Conference on Electrical Contacts*, p. 313, AMP Incorporated , Harrisburg, Pennsylvania (1989).
18. T. D. Ibragimov, A. R. Imamaliyev, and G. M. Bayramov "*Peculiarities of electro-optic properties of the ferroelectric particles-liquid crystal colloids*", AIP Conference Proceedings **1727**, 020011 (2016).
19. N. E. Grzeskowiak and J. F. Winkel, *J. Electrochem. Soc.* **154**, J289 (2007).
20. R. Withnall, J. Silver, T. G. Ireland, G. R. Fern, and P. J. Marsh, *J. Electrochem. Soc.* **156**(11) J326 (2009).